Glass Transition Temperature Depression of Elastomers Blended with Poly(propene)s of Different Stereoregularities

Dietmar Mäder,[†] Matthias Bruch,[†] Ralph-Dieter Maier,[†] Florian Stricker,[‡] and Rolf Mülhaupt*,[†]

Freiburger Materialforschungszentrum und Institut für Makromolekulare Chemie der Albert-Ludwigs-Universität, Stefan-Meier-Str. 21, D-79104 Freiburg i. Br., Germany, and TARGOR GmbH, Anwendungstechnik, F206, D-67056 Ludwigshafen, Germany

Received July 21, 1998; Revised Manuscript Received November 13, 1998

ABSTRACT: Glass temperature depression, measured by means of dynamic mechanical analysis, of elastomers blended together with isotactic, syndiotactic, and atactic poly(propene), PP, was detected for the first time. Two-phase melt blends consisting of PP and elastomers such as polystyrene-*block*-poly(ethene-*co*-1-butene)-*block*-polystyrene, SEBS, and poly(ethene-*co*-1-octene), EO, were prepared. The depression of the glass temperature, T_g, of PP/elastomer blends with respect to the T_g of the corresponding neat elastomer was attributed to thermally induced internal stress resulting from differential volume contraction of the two phases during cooling from the melt. The temperature dependence of the specific volume of the blend components was determined by pressure−volume−temperature measurements. The specific volume of the blend components was measured at temperatures varying between 30 and 270 °C and extrapolated to the elastomer T_g at −50 °C. This stress accumulation, reflected by glass temperature depression, is likely to influence mechanical properties, especially impact strength of PP/elastomer blends.

Introduction

Various polymers are frequently blended together in order to combine the properties of the individual components.[1] An important objective is to improve toughness of polymers by dispersing elastomers in the polymer matrix.[2] Impact properties of such blends are mainly governed by the morphology which is characterized by particle size, interparticle distance, and interfacial properties, i.e., interfacial adhesion. Increased toughness results from superposition of local stress fields arising from the dispersed particles.[3−5] Thermal properties of such blends, i.e., glass transition temperature (T_g) and melting temperature (T_m), are of particular interest. Blends consisting of semicrystalline polymers can exhibit a depression of T_m.[6,7] Concerning T_g it is accepted that two single T_g's are observed for immiscible blends and a single T_g for miscible blends.[8,9] Compatibility of the components, i.e., partial miscibility, is reflected by the presence of two T_g's in the blend, which are shifted toward each other; i.e., the higher T_g is lowered and the lower T_g is increased simultaneously. However, a depression of the lower T_g has not been reported for nonreactive polymer blends. Such negative T_g shifts of the dispersed phases ranging up to −12 °C have been only observed for ABS.[5,10,11] ABS consists of a continuous poly(styrene-*co*-acrylonitrile) (SAN) matrix containing dispersed polybutadiene particles (PB), embedded in a shell containing covalently attached SAN. Thermal stress[12−14] can arise from the thermal history of the blend and is attributed to differences in thermal expansion of the blend components. It is assumed that in ABS the thermal stress is completely transferred across the matrix/elastomer interface, due to good adhesion between SAN-grafted PB particles and SAN matrix. Stress transfer is promoted by either covalent interfacial bonds or van der Waals interactions. The role of interfacial adhesion requires further investigation. It still has to be clarified whether interfacial adhesion or rather covalent interfacial coupling is a crucial prerequisite for stress transfer.

There is no systematic investigation available concerning the influence of the elastomer/matrix interface, i.e., interfacial adhesion, particle size, or volume fraction on T_g of the dispersed nonreactive elastomer. Therefore, the T_g's of various elastomers in melt blends of poly(propene)s (PP) with different stereoregularity were studied by means of dynamic mechanical analysis (DMA) in order to examine the negative T_g shift in such nonreactive melt blends. Accordingly, melt blends of isotactic (iPP), syndiotactic (sPP), and high molecular weight atactic poly(propene) (aPP) with elastomers such as polystyrene-*block*-poly(ethene-*co*-1-butene)-*block*-polystyrene (SEBS) and poly(ethene-*co*-1-octene) (EO) were prepared. Blends of PP with different stereoregularities and different elastomers represent model systems for the study of the influence of matrix/elastomer adhesion on T_g as well as the influence of elastomer volume fraction on T_g. Mismatch between thermal expansion of the matrix and of the elastomer is expected to account for thermally induced stress. Therefore, the temperature dependence of the specific volumes of the blend components was determined by means of pressure−volume−temperature (PVT) measurements.

Experimental Section

Materials. The polymers used in this study and their physical properties are shown in Table 1. Most polymers were of commercial grade and used without further purification. Metallocene-based iPP, Novolen M (MFI = 4 g/10 min at 200 °C), was supplied by BASF AG, whereas metallocene-based sPP, sPH40, was supplied by Mitsui. Metallocene-based high molecular weight aPP was provided by Suhm.[15] The conventional Ziegler-based PP's TM6100K, KM6100 and JE6100 (PP214, PP286, PP394), and SEBS (Kraton) were supplied by Shell. The two SEBS types used in this study had a polystyrene/

* To whom correspondence should be addressed.
[†] Albert-Ludwigs-Universität.
[‡] TARGOR GmbH.

10.1021/ma981154q CCC: $18.00
Published on Web 02/04/1999

Table 1. Abbreviations and Physical Properties of the Polymers Used

abbr	commercial name	polymer	polymerization	M_w[a] (kg/mol)	M_w/M_n[a]	η_0[b] (kPa s)	T_g[c]/T_m[d] (°C)	ΔH_m[d] (J/g)	T_{cr}[d] (°C)	tacticity[e] (%)	density[f] (g/cm^3)	DC[g] (%)
iPP	Novolen M (BASF)	i-PP	metallocene	267.0	2.3	4.8	6.2/149.5	84.5	95.4	95 (mm)	0.904	62.8−56.3
sPP	sPH40 (Mitsui)	s-PP	metallocene	150.9	1.9	9.0	11.0/116.5, 130.0	33.7	61.4	91 (rr)	0.880	18.0
aPP	JS69 (our laboratory)	a-PP	metallocene	357.9	1.7	7.0	4.7			13.5 (mmmm)	0.856	
PP214	TM6100K (Shell)	i-PP	Ziegler	214.1	4.5	7.7	10.7/170.0	102.8	99.4	98 (mm)	0.904	62.8−56.3
PP286	KM6100[h] (Shell)	i-PP	Ziegler	285.9	4.9	40.6	10.7/172.8	101.4	96.9	97 (mm)	0.905	64.0−57.3
PP394	JE6100 (Shell)	i-PP	Ziegler	394.3	4.1	66.2	10.6/171.5	102.6	96.9	97 (mm)	0.905	64.0−57.3
SEBS	Kraton G1652 (Shell)	SEBS[i]	anionic	87.1	1.04	130.4	−45.4				0.906	
SEBS$_f$	Kraton FG1901X (Shell)	SEBS-*g*-MA[i,j]	anionic	97.7	1.15		−44.3					
EO	Engage 8150 (Dow Chemical)	EO[k]	metallocene	162.1	2.1	88.0	−42.9/59.2	55.1	32.9		0.868	

[a] Determined by GPC based on polystyrene standards for SEBS (high-temperature GPC based on PP and PE standards for PP's and EO, respectively). [b] Zero shear viscosity η_0 from dynamic experiments at 200 °C [c] Determined by DMA at a heating rate of 2 K/min. [d] Determined by DSC at a heating rate of 10 K/min (T_m) and at a cooling rate 30 K/min (T_{cr}). [e] Determined by ^{13}C NMR by triad or pentad distribution. [f] Measured with a micropycnometer at 25 °C and taken as the reference for PVT measurements. [g] Degree of crystallinity (DC) was calculated using $\rho_{iPP,100\%} = 0.936-0.946$ g/cm^3, $\rho_{iPP,0\%} = 0.850$ g/cm^3, $\rho_{sPP,100\%} = 0.989$ g/cm^3, and $\rho_{sPP,0\%} = 0.856$ g/cm^3. [h] Contains 4.11% atactic PP (extractable with xylene). [i] Polystyrene-*block*-poly(ethene-*co*-1-butene)-*block*-polystyrene triblock copolymer (S:EB:S = 1:5:1) containing 36 wt % 1-butene. [j] Contains 2 wt % maleic anhydride. [k] Contains 25 wt % 1-octene.

poly(ethene-*co*-1-butene) weight ratio of 29 wt %/71 wt % (Kraton G1652) and 28 wt %/72 wt % (Kraton FG1901X), respectively. Kraton FG1901X contained additionally 2 wt % maleic anhydride (MA) which was melt-grafted onto its EB block. The metallocene-based EO rubber contained 25 wt % 1-octene (Engage 8150) and was supplied by Dow Chemical.

Melt Blending. PP/elastomer melt blends usually containing 20 vol % elastomer were prepared by different blending methods. In all cases 0.5 wt % Irganox 1010/Irgafos 168 (80 wt %/20 wt %) was added as stabilizers. Extruder blends were prepared in a twin-screw extruder (ZSK25, Werner & Pfleiderer) with 300 rpm and a maximum temperature of 230 °C as reported elsewhere in more detail.[16] The extruded blends and the pure Ziegler-based PP's were injection molded to obtain specimens for DMA measurements. Kneader blends were prepared in a Haake Rheomix 90 twin-screw kneader equipped with a 60 mL mixing chamber preheated at 200 °C and operated at 60 rpm. The chamber was always filled with 45 mL of polymer. First iPP was molten together with the stabilizers for 90 s. Then the elastomer was added within 30 s. After further 180 s (total mixing time was 300 s), the sample was quickly recovered and quenched between cooled metal plates. Melt blends containing aPP (sPP) were prepared using a microcompounder (Daca Instruments) equipped with a 5 mL mixing chamber preheated at 200 °C and operated at 60 rpm. Two milliliters of aPP/elastomer (3 mL of sPP/elastomer) was molded in the presence of stabilizers for 300 s. Then the sample was quickly recovered and quenched between cooled metal plates. Rectangular bars of 50 × 6 × 2 mm for DMA measurements were compression molded in an evacuated press (Schwabenthan Polystat 100) by annealing at 200 °C for 10 min and quenching to ambient temperatures.

Thermal Analysis. Differential scanning calorimetry (DSC) measurements were performed on a Perkin-Elmer DSC-7. Melting temperatures (T_m) and melting enthalpies (ΔH_m) were determined at a heating rate of 10 K/min. Crystallization temperatures (T_{cr}) were determined at a cooling rate of 30 K/min.

Dynamic Mechanical Analysis (DMA). Glass transition temperatures were determined by dynamic mechanical analysis on a Rheometrics Solids Analyzer RSA II at 1 Hz and a heating rate of 2 K/min using a dual cantilever geometry (50 × 6 × 2 mm) and a strain of 0.2%. The storage (E') and loss moduli (E'') and the loss tangent (tan(δ)) were measured from −100 °C up to temperatures accessible with dual cantilever geometry.

Transmission Electron Microscopy (TEM). TEM measurements were performed on a Zeiss CEM 902 transmission electron microscope applying an acceleration voltage of 80 kV. The samples were ultramicrotomed at −120 °C (Ultracut E, Reichert & Jung, equipped with a diamond knife). Ultrathin sections of approximately 80 nm were stained with gaseous RuO_4 prepared from 10 mg of $RuCl_3$ and 1 mL of 10 wt % NaOCl solution. The diameters of approximately 1500 particles were measured from TEM images and subjected to a regularization procedure in order to calculate the corrected average particle size as described elsewhere.[16]

Density and Pressure−Volume−Temperature (PVT) Measurements. Polymer densities were measured at 25 °C and atmospheric pressure using a Quantachrome micropycnometer (Boynton Beach, FL). According to literature procedures,[17] the degree of crystallinity (DC) was calculated using the values $\rho_{iPP,100\%} = 0.936-0.946$ g/cm^3, $\rho_{iPP,0\%} = 0.850$ g/cm^3, $\rho_{sPP,100\%} = 0.989$ g/cm^3, and $\rho_{sPP,0\%} = 0.856$ g/cm^3, respectively.[18,19] Volume changes as a function of temperature and pressure were measured by means of a Gnomix PVT apparatus (Boulder, CO).[20] The sample cell contained about 1 g of polymer sample and mercury as confining fluid. Measurements were performed in the isothermal mode; i.e., the sample was maintained at a given temperature, while the pressure was continuously raised from 10 to 200 MPa, pressure, volume, and temperature being recorded in steps of 10 MPa. The specific volume v_{sp} corresponding to $p = 0$ MPa (set as atmospheric pressure) was then extrapolated using the Tait equation[21] implemented in the PVT software. Subsequently, this procedure was repeated for all isotherms between 30 and 270 °C in steps of approximately 10 °C. v_{sp} was evaluated from the resulting zero pressure isobar. The sensitivity of the Gnomix apparatus is of 0.0002 cm^3/g, whereas the absolute accuracy is of 0.002 cm^3/g in the low-temperature range ($T <$ 200 °C) and better than 0.004 cm^3/g at higher temperatures.[22] To evaluate v_{sp} at a given temperature, e.g. 95 °C, the values of v_{sp} were linearly interpolated between the corresponding measured temperatures.

PVT data at $p = 0$ MPa were used since DMA measurements were also performed at atmospheric pressure. It should

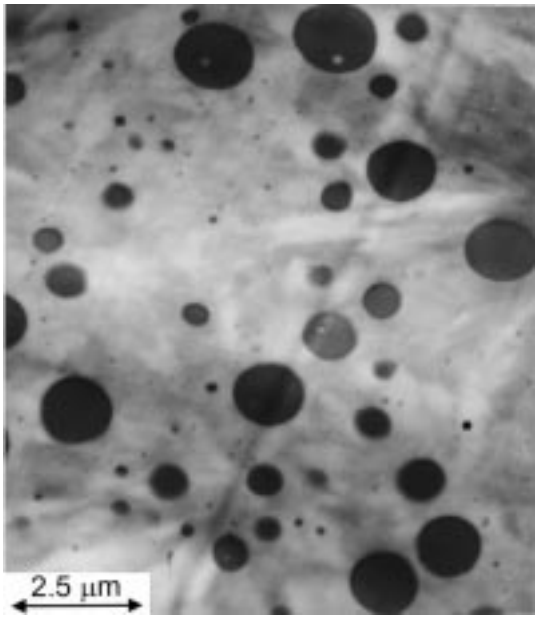

Figure 1. TEM micrograph of the blend iPP−EO20 (dark spots can be assigned to dispersed EO).

be mentioned that the T_g strongly depends on pressure.[8,9,23]

Results and Discussion

Morphology. The morphology of immiscible polymer blends depends on the volume fraction of the dispersed phase. At low elastomer volume fractions ranging from $0 < \Phi < 20$ vol %, a spherical morphology of the dispersed phase was observed. A TEM micrograph of an iPP−EO blend containing 20 vol % EO is shown in Figure 1. This is in accordance with earlier observation by Stricker,[16] who investigated i-PP/SEBS blends. T_g was determined by means of DMA where T_g corresponds to the maximum of the tan(δ) curve. Table 1 summarizes the T_g's of both the matrix (M) polymers (T_g^M) and of the elastomer (E) phases (T_g^E). Table 2 shows the T_g's of the studied blends.

Influence of Elastomer Type. In this study two different elastomers were used. SEBS, an elastomer of narrow molecular weight distribution (MWD) obtained by anionic polymerization, is regarded as a monodisperse model elastomer showing negligible effects due to broad MWD. Furthermore, SEBS is a thermoplastic elastomer, physically cross-linked by the PS end blocks. In addition to SEBS, EO was used as a representative of the polymer class of ethene/1-olefin rubbers or elastomers, frequently employed in polymer blends as toughening agents. Due to the single-site nature of metallocene catalysts, ethene/1-octene copolymers with polydispersities of approximately 2 can be produced. Both elastomers exhibit a similar T_g of about −45 and −43 °C, respectively, as determined by DMA.

Tables 1 and 2 show the T_g's of the components SEBS and EO and of the blends iPP−SEBS20 and iPP−EO20. In both blends the T_g of the dispersed elastomer phase $T_g^E(\Phi)$ is depressed when compared to the T_g^E of the bulk elastomer. This depression ΔT_g^E at an elastomer volume fraction Φ is defined as

$$\Delta T_g^E(\Phi) = |T_g^E| - |T_g^E(\Phi)| \quad (1)$$

For both iPP blends $\Delta T_g^E(\Phi=20)$ is in the range of −7 °C. Both elastomer types exhibit similar thermal behavior; i.e., there is no significant influence of the type of elastomer on $\Delta T_g^E(\Phi=20)$. The T_g^M of the iPP matrix remains unchanged at about 6 °C.

For the study of the influence of functionalization, i.e., different interfacial adhesion, melt blends of iPP with functionalized SEBS grafted with 2 wt % MA ($SEBS_f$) and unfunctionalized SEBS were prepared. In Figure 2 DMA traces of SEBS, $SEBS_f$, iPP−SEBS20, and iPP−$SEBS_f$20 are presented.

The shift of T_g^E toward lower temperatures is approximately the same for both iPP−SEBS20 and iPP−$SEBS_f$20. All iPP melt blends ($\Phi = 20$) show a $\Delta T_g^E \approx -7$ °C. Thus, for these blends no significant influence of the type of elastomer, i.e., SEBS, EO, and $SEBS_f$, on T_g^E depression can be observed. In another work it was shown, however, that adhesion between $SEBS_f$ and isotactic poly(propene) (PP286) is significantly decreased by the MA functionalization of SEBS.[24] From the peel strength of PP286/SEBS being higher than that of PP286/$SEBS_f$, it was thus concluded that MA functionalization reduces interaction between $SEBS_f$ and PP. Although SEBS and $SEBS_f$ exhibit different adhesion toward iPP, the same $\Delta T_g^E(\Phi=20)$ is detected in these blends. Also, no significant difference for $\Delta T_g^E(\Phi=20)$ can be observed in the sPP blends, i.e., sPP−SEBS20 and sPP−$SEBS_f$20. This again indicates that different interaction of matrix/elastomer has no significant influence on ΔT_g^E.

Influence of Elastomer Particle Size. To study the influence of the particle size of the dispersed elastomer on ΔT_g^E, blends of Ziegler-based PP's having different molecular weights with 15 vol % SEBS were prepared. By varying the molecular weight of the PP's, different viscosity ratios with SEBS were achieved. Thus, the SEBS particle size was varied between 260 and 500 nm at a constant SEBS volume fraction. These samples were taken from another study.[16] In Figure 3 DMA traces of these blends are depicted.

The molecular weight of the PP sample is indicated by the number and the average SEBS particle size is indicated by a subscript; e.g., sample PP214−$SEBS_{500}$ represents a blend consisting of the PP214 with 15 vol % SEBS with a mean particle size of 500 nm. It can be seen that the maximum in tan(δ) varies between −51 and −53 °C; thus, ΔT_g^E is in the range of −5 to −7 °C. This small difference indicates that the influence of particle size on ΔT_g^E is only marginal.

Influence of PP Stereoregularity. Figure 4a exhibits the DMA traces of the blends of sPP and aPP with SEBS and Figure 4b the blends with EO. Blends of iPP with SEBS and EO are shown in Figure 2 and Figure 5. The $\Delta T_g^E(20)$ data are summarized in Table 2. The value of ΔT_g^E is larger for the semicrystalline iPP and sPP and lower for the complete amorphous aPP. This implies that ΔT_g^E depends on the stereoregularity or the crystallinity, respectively. The magnitude of ΔT_g^E decreases with decreasing degree of crystallinity (DC(iPP) > DC(sPP) > DC(aPP)).

These observations rise the question whether different interfacial adhesion or rather different crystallinity accounts for ΔT_g^E. According to Lohse et al.,[25] iPP and aPP are completely miscible in the melt, whereas iPP and sPP are immiscible in the melt.[26] This implies that SEBS and EO exhibit different interfacial tension toward iPP/aPP and sPP in the melt and different interfacial adhesion in the solid state. Therefore, elastomer blends with iPP and aPP should have similar

Table 2. Glass Transition Temperatures of Matrices (M) T_g^M and Elastomer (E) T_g^E As Measured by DMA and T_g Depression ΔT_g^E of the Blends Studied

abbreviation	preparation[a]	M	E	Φ (vol %)	T_g^E (°C)[b]	T_g^M (°C)[b]	ΔT_g^E (°C)	particle size (nm)
PP214−$SEBS_{500}$	Ex/IM	PP214	SEBS	15	−52.7	11.1	−7.3	500
PP286−$SEBS_{290}$	Ex/IM	PP286	SEBS	15	−50.6	10.9	−5.2	290
PP394−$SEBS_{260}$	Ex/IM	PP394	SEBS	15	−51.9	10.9	−6.5	260
PP286−SEBS20−IM	Ex/IM	PP286	SEBS	20	−51.5	7.6	−6.1	
PP286−SEBS20−CM	K/CM	PP286	SEBS	20	−53.0	7.4	−7.6	
iPP−SEBS20	K/CM	iPP	SEBS	20	−52.9	6.1	−7.5	
iPP−$SEBS_f$20	K/CM	iPP	$SEBS_f$	20	−51.3	6.0	−7.0	
iPP-EO5	K/CM	iPP	EO	5	−57.0	6.3	−14.1	220
iPP-EO10	K/CM	iPP	EO	10	−55.1	6.4	−12.2	220
iPP-EO15	K/CM	iPP	EO	15	−53.0	6.4	−10.1	240
iPP-EO20	K/CM	iPP	EO	20	−50.5	6.6	−7.6	310
iPP-EO40	K/CM	iPP	EO	40	−47.7	6.1	−4.8	
sPP−SEBS20	K/CM	sPP	SEBS	20	−51.7	9.9	−6.3	
sPP−$SEBS_f$20	mC/CM	sPP	$SEBS_f$	20	−50.2	9.9	−5.9	
sPP-EO20	mC/CM	sPP	EO	20	−51.4	9.1	−8.5	
aPP−SEBS20	mC/CM	aPP	SEBS	20	−50.1	3.9	−4.7	
aPP-EO20	mC/CM	aPP	EO	20	−48.5	4.6	−5.6	

[a] Prepared with extruder (Ex), kneader (K), and microcompounder (mC); DMA specimens were injection (IM) or compression molded (CM). [b] Determined by DMA at a heating rate of 2 K/min.

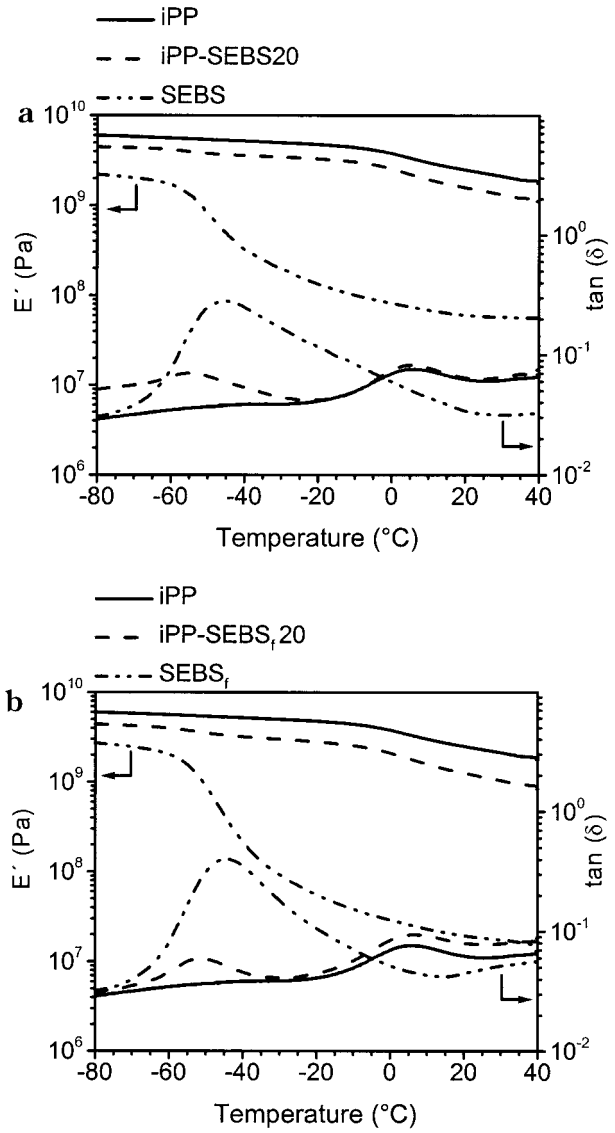

Figure 2. DMA traces of metallocene−iPP/SEBS blends with Φ =20 vol % (iPP, SEBS, $SEBS_f$, iPP−SEBS20, iPP−$SEBS_f$20). T_g is assigned to the maximum of the tan(δ) curve.

ΔT_g^E whereas the corresponding blends based upon sPP should give different ΔT_g^E when assuming that T_g is influenced exclusively by interfacial adhesion. However,

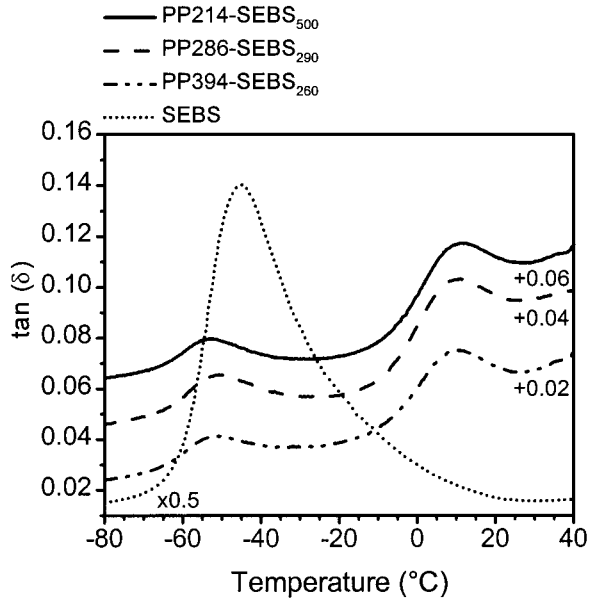

Figure 3. DMA traces of Ziegler−PP/SEBS blends (Φ = 15 vol %) having different elastomer particle sizes (PP214−$SEBS_{500}$, PP286−$SEBS_{290}$, PP394−$SEBS_{260}$). (The tan(δ) curves are vertically shifted as denoted.)

the value of ΔT_g^E decreases in the order iPP > sPP > aPP. This indicates that PP matrix crystallinity is crucial to ΔT_g^E, whereas interfacial adhesion is much less important. In accordance to this hypothesis, similar ΔT_g^E are found for SEBS and $SEBS_f$ which exhibit substantially different interfacial adhesion with respect to i-PP. Both metallocene-based iPP and Ziegler-based i-PP give very similar ΔT_g^E. There is a marginal influence of the preparation method on ΔT_g^E when comparing injection molding (IM) vs compression molding (CM) as evidenced for PP286−SEBS20−IM and PP286−SEBS20−CM.

Influence of Elastomer Volume Fraction. To study the influence of the elastomer volume fraction Φ on ΔT_g^E in iPP/EO blends, the EO content Φ was varied from 5 to 10, 15, 20, and 40 vol %. Figure 5 shows the DMA traces of iPP/EO blends containing different amounts of EO. Apparently $\Delta T_g^{EO}(\Phi)$ depends strongly on Φ. The highest value of ΔT_g^{EO} is observed for the lowest Φ = 5 vol %. With increasing EO volume fraction the value of ΔT_g^{EO} decreases.

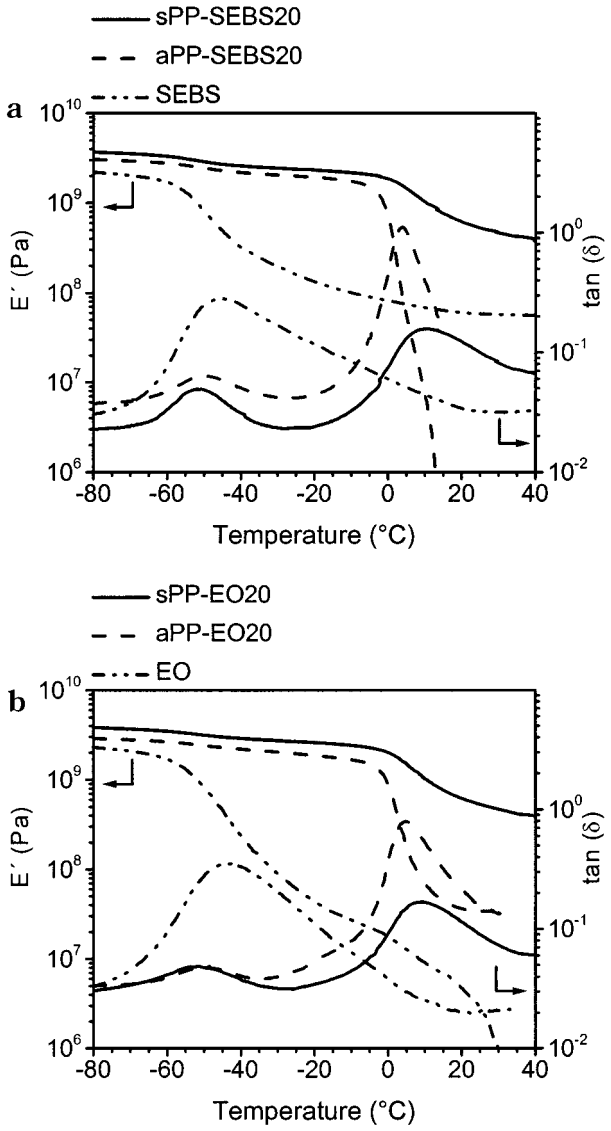

Figure 4. DMA traces of sPP and aPP blends with SEBS and EO ($\Phi = 20$ vol %): (a) sPP−SEBS20, aPP−SEBS20; (b) sPP−EO20, aPP− EO20.

Since all blends containing less than 20 vol % exhibit comparable particle sizes of the dispersed EO, the elastomer particle size does not affect the $\Delta T_g^{EO}/\Phi$ dependence significantly. The stiffness of the blends reflected by the decreasing storage moduli $E'(T_g^E = -50$ °C) with increasing Φ appears to play a key role.[13] With increasing Φ, E' of the blend decreases steadily in comparison to E' of the matrix as depicted in Table 3.

DMA measurements show that the influence of the elastomer type—associated with the interfacial adhesion between elastomer and PP of different stereoregularities—on ΔT_g^E is only marginal. However, matrix stereoregularity corresponding to the degree of crystallinity influences the magnitude of ΔT_g^E. Moreover, $\Delta T_g^E(\Phi)$ is strongly affected by the elastomer volume fraction Φ.

PVT Measurements. ΔT_g^E has not been observed for nonreactive blends yet. A negative ΔT_g^E is observed for ABS systems[11] for which the decay of the elastomer T_g is explained in terms of different thermal expansion between matrix and elastomer, thus producing thermal stress.[12,13,27] Therefore, it is important to quantify thermal expansion or contraction of the investigated blend components. The temperature dependence of the

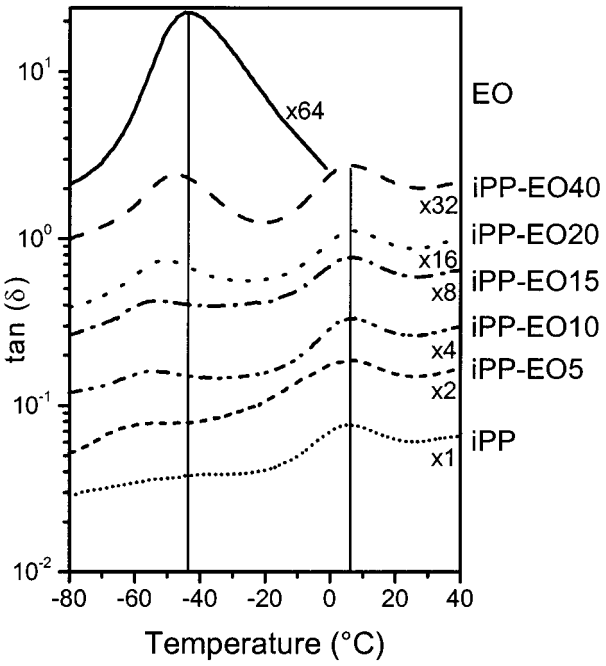

Figure 5. tan(δ) of iPP/EO blends with different volume fractions $\Phi_{EO} = 5$, 10, 15, 20, and 40 vol %. The vertical lines indicate T_g^{iPP}(bulk) and T_g^{EO}(bulk). (The tan(δ) curves are vertically shifted by factors as denoted.)

Table 3. Storage Moduli at −50 °C, $E'(-50$ °C), of the Blends iPP/EO As Measured by DMA

sample	$E'(-50$ °C) (GPa)	sample	$E'(-50$ °C) (GPa)
iPP	5.41	iPP−EO20	3.39
iPP−EO5	4.97	iPP−EO40	2.80
iPP−EO10	3.98	EO	0.84
iPP−EO15	3.67		

specific volumes v_{sp} of the matrix PP's and of SEBS and EO was determined by PVT measurements. The v_{sp} vs temperature functions of iPP, sPP, and aPP with temperatures ranging from 30 to 270 °C at $p = 0$ MPa are shown in Figure 6a.

In the melt state the v_{sp}'s of all three PP's are of the same order of magnitude. iPP and aPP show almost the same v_{sp} traces, whereas sPP exhibits a slightly higher v_{sp}[26,28] which may be attributed to different conformations of the sPP chains in the melt compared to those of aPP or iPP. In the semicrystalline region both iPP and sPP show large differences of v_{sp} compared to v_{sp} in the melt. Since the Gnomix apparatus allows only to measure v_{sp} at temperatures higher than 30 °C, v_{sp} values for lower temperatures have been extrapolated. The extrapolation of v_{sp} from 30 to 0 °C (T_g^{PP}) and subsequently to −50 °C (T_g^E) for the PP's is described in the Appendix. The v_{sp} values are summarized in Table 4.

In Figure 6b the PVT data of the elastomers SEBS and EO are presented. SEBS shows a continuous decrease of v_{sp} with decreasing temperature. No significant change in slope in the v_{sp} vs temperature curve is detectable at 100 °C, although this corresponds to the T_g of the PS block in SEBS. The PVT data are listed in Table 4.

In Figure 7 the difference in volume contraction of the matrix and dispersed phase during cooling from the melt is demonstrated for the system iPP/SEBS. In Figure 7a,b the v_{sp} vs temperature dependencies of the bulk components are displayed. The extrapolation of v_{sp}

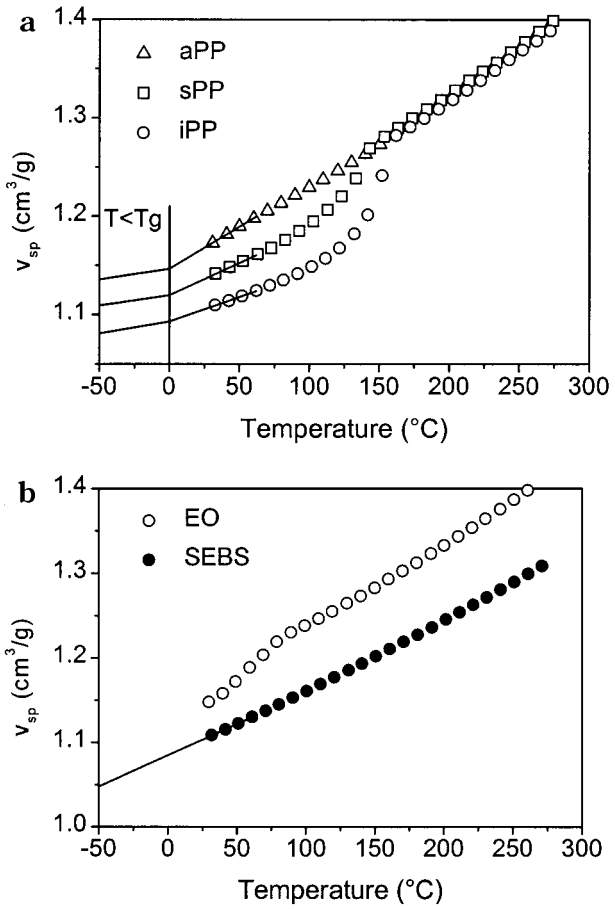

Figure 6. Specific volume v_{sp} vs temperature of the bulk components as measured by PVT ($p = 0$ MPa) and extrapolated to −50 °C. (a) Matrices: aPP, sPP, and iPP. (b) Elastomers: EO and SEBS.

Table 4. Specific Volumes v_{sp} of the Bulk Polymers As Measured by PVT

bulk polymer	v_{sp} (cm^3/g) at 200 °C[a]	95 °C[a]	60 °C[a]	30 °C[a]	0 °C[b]	−50 °C[b]
iPP	1.3160	1.1438	1.1229	1.1083	1.0930	1.0810
sPP	1.3239	1.1867	1.1523	1.1393	1.1196	1.1094
aPP	1.3192	1.2254	1.1963	1.1719	1.1464	1.1357
SEBS	1.2440	1.1564	1.1216	1.1074	1.0849	1.0479
EO	1.3323	1.2348	1.1895	1.1481		

[a] Determined by PVT measurements. [b] Extrapolated according to the Appendix.

of iPP and SEBS to −50 °C is adapted from Figure 6 according to the procedure described in the Appendix. The v_{sp} difference in the temperature range $T_{cr}^{M} = 95$ °C and $T_g^{E} = -50$ °C for iPP and SEBS is denoted Δv_{sp}(iPP) and Δv_{sp}(SEBS), respectively. The difference between Δv_{sp}(SEBS) and Δv_{sp}(iPP) is denoted $\Delta(\Delta v_{sp})$. To demonstrate $\Delta(\Delta v_{sp})$ in Figure 7c, the v_{sp}(iPP) curve is shifted to superimpose to v_{sp}(SEBS) at $T_{cr}^{iPP} = 95$ °C. $\Delta(\Delta v_{sp})$ is the volume dilatation of the dispersed elastomer, i.e., an additional volume which is occupied by the elastomer. In Table 5 the $\Delta(\Delta v_{sp})$ for different temperature regimes is listed, from T_{cr}^{M} to 30 °C (regime I), from 30 to 0 °C (T_g of PP, regime II), and from 0 to −50 °C (T_g of SEBS, regime III).

In the temperature regime III $\Delta(\Delta v_{sp})$ is of about 0.026 cm^3/g for all PP's. Differences due to crystallinity occur in the regimes I and II. The main contribution to $\Delta(\Delta v_{sp})$ arises in the temperature regime III, i.e., between T_g^{PP} and T_g^{SEBS}.

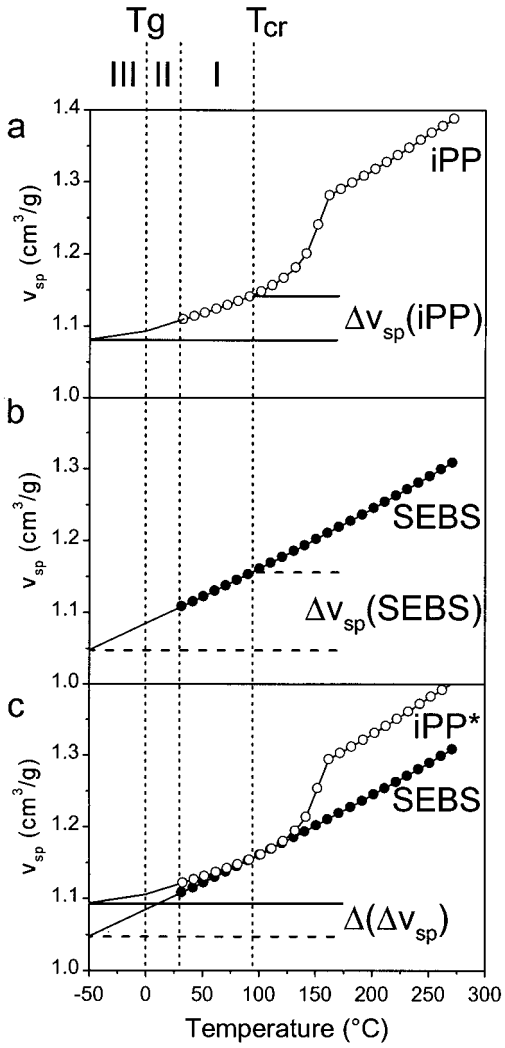

Figure 7. Specific volume v_{sp} vs temperature of iPP (a) and SEBS (b). Difference in v_{sp} between $T_{cr}^{iPP} = 95$ °C and $T_g^{SEBS} = -50$ °C is indicated by solid (iPP) and dashed (SEBS) lines. To visualize $\Delta(\Delta v_{sp}) = \Delta v_{sp}$(SEBS) − Δv_{sp}(iPP) (c) the v_{sp}(iPP) is shifted to superimpose to v_{sp}(SEBS) at $T_{cr}^{iPP} = 95$ °C (v_{sp}(iPP*)). $\Delta(\Delta v_{sp})$ is indicated by solid/dashed lines. The dotted lines divide the temperature regimes: T_{cr}^{iPP} to 30 °C (regime I), from 30 to 0 °C (T_g of PP, regime II), and from 0 to −50 °C (T_g of SEBS, regime III). (a) iPP. (b) SEBS. (c) iPP* and SEBS.

Table 5. Volume Dilatation $\Delta(\Delta v_{sp})$ of SEBS in Blends with PP's within Different Temperature Regimes ($\Delta(\Delta v_{sp}) = \Delta v_{sp}$((SEBS) − Δv_{sp}(PP))

regime	temp range	$\Delta(\Delta v_{sp})$ (cm^3/g) iPP/SEBS[a]	sPP/SEBS[b]	aPP/SEBS[c]
I	T_{cr} to 30 °C[d]	0.0135	0.0012	
II	30 °C to T_g^{PP}	0.0072	0.0028	
III	T_g^{PP} to T_g^{SEBS}	0.0250	0.0268	0.0263
sum	T_{cr} to T_g^{SEBS}	0.0457	0.0308	0.0263

[a] T_{cr}(iPP) = 95 °C, T_g(iPP) = 0 °C, T_g(SEBS) = −50 °C. [b] T_{cr}(sPP) = 60 °C, T_g(sPP) = 0 °C, T_g(SEBS) = −50 °C. [c] T_g(aPP) = 0 °C, T_g(SEBS) = −50 °C. [d] Lowest accessible temperature for PVT measurement.

In comparison to the bulk elastomer, the bulk PP exhibits a different volume contraction. In the blend the difference in volume contraction between matrix and dispersed elastomer phase leads to stress accumulation starting from the temperature at which the morphology is frozen, meaning the matrix has reached the solid state. For iPP and sPP this solidification temperature corresponds to the crystallization temperature (95 and

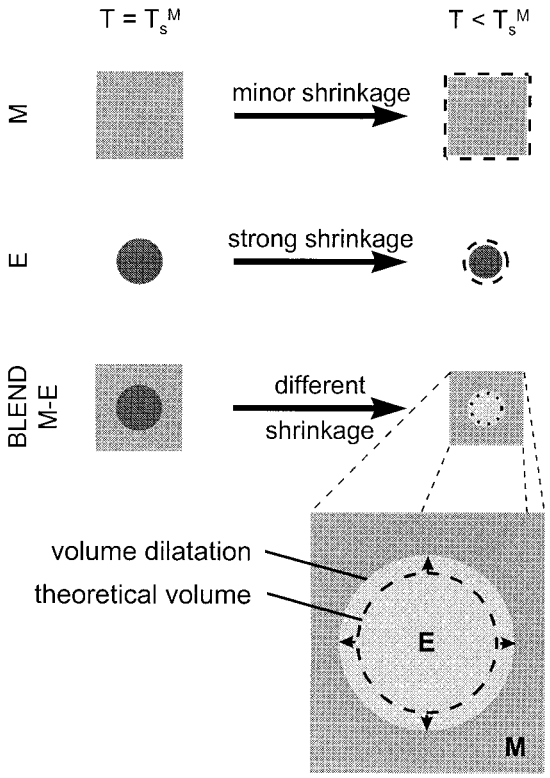

Figure 8. Model of thermal behavior of dispersed E in matrix M. Volume of matrix M (bulk), phase E (bulk), and blend M−E with dispersed E is shown at temperatures $T = T_S^M$ and $T < T_S^M$. Differences in thermal shrinkage between M and E are the origin of volume dilatation in dispersed E.

60 °C, respectively, as determined by DSC at a cooling rate of 30 K/min during melt cooling), whereas for aPP the morphology is frozen at its $T_g = 0$ °C. Starting from these temperatures, the embedded elastomer tends to shrink more strongly than the matrix. This difference in volume contraction in the blend cannot be compensated macroscopically. Consequently, the surrounding matrix forces the elastomer particles to occupy a larger volume than the volume that corresponds to bulk elastomer under the same thermal conditions. This is equivalent to a volume dilatation of the dispersed elastomer phase in the blend. Such volume dilatation can be detected macroscopically as a T_g shift. Volume dilatation means a reduced density of the elastomer; thus, a depression of T_g will be observed in comparison to the bulk elastomer.[29]

In general, little attention has been paid to the thermal properties of such dispersed elastomers. It may be assumed that thermal stress influences the mobility of polymers and consequently their T_g. In the temperature range between T_{cr}^M (T_g^M) and T_g^E the shrinkage of the matrix is significantly smaller than that of the still molten elastomer phase. If the interaction between dispersed particles and the matrix is strong enough to prevent debonding, a thermally induced stress develops in the particle; i.e., a volume dilatation of the dispersed elastomer particles occurs. Therefore, a negative shift of the elastomer T_g offers macroscopic evidence for thermally induced microscopic stresses.

In Figure 8 a model of the thermal behavior of a thermoplastic blend during cooling from the melt is proposed. The matrix solidifies at the temperature T_S^M which is equal to T_{cr}^M for a semicrystalline material (M) and T_g^M for amorphous M. The other blend component (E) has a lower T_S^E than M. The volume of bulk M, of bulk E, and of the corresponding blend M−E is shown schematically for $T = T_S^M$ and $T < T_S^M$. Above the solidification temperature $T > T_S^M$, M and the dispersed E particles occupy a certain volume according to their mass fraction in the blend. Differences in $v_{sp}(M)$ and $v_{sp}(E)$ are compensated by macroscopic expansion or contraction of the melted blend. Upon cooling from the melt M solidifies at T_S^M. At further cooling the difference in volume changes, i.e., different $\Delta v_{sp}(E)$ and $\Delta v_{sp}(M)$, cannot be compensated macroscopically any more. The volume contraction of M is smaller than that of E, i.e., $\Delta v_{sp}(M) < \Delta v_{sp}(E)$. Thus, at $T < T_S^M$ the surrounding matrix M imposes to the E particles a certain volume that is larger than the respective $v_{sp}(E)$ of bulk E. The particle volume of E is governed by M, which means that the E particles are forced to adapt to the $v_{sp}(M)$, i.e., E is dilated.

It must be stated that in this model volume contraction during the crystallization process of semicrystalline polymers, such as iPP, is not taken into account. It is known that negative pressure effects can occur during isothermal crystallization of iPP.[30] These negative pressure effects can lead to hole formation in thin films or cavities in bulk. A similar effect can be observed during crystallization at incompatible i-PP interfaces. As described by Wool, influx formation appears at interfaces of i-PP and HDPE or LLDPE during crystallization.[31] Intra- or interspherulitic entrapments can be formed. These effects may also occur during quenching. This additional contribution may amplify the volume dilatation of the elastomer particles in the studied blends.

Conclusions

Research on impact-modified blends is mainly focused on determination of structure−property relationships. Besides morphological parameters, research is focused on interfacial properties, e.g. interfacial adhesion. It is believed that improved interfacial adhesion between elastomer and matrix is a main prerequisite for optimized impact properties. Induced thermal stresses may give additional contribution to the development of stress fields around the dispersed particles which contribute to mechanical, i.e., especially impact properties of blends.

Melt blends of PP of different stereoregularities with elastomers exhibiting spherical morphology were prepared. It was shown that the dispersed particles show a depressed T_g^E with respect to the bulk component. The extent of this T_g depression ΔT_g^E depends on the elastomer volume fraction and the type of matrix. The value of ΔT_g^E increases with increasing crystallization temperature and increasing degree of crystallinity of the matrix. This ΔT_g^E is attributed to volume dilatation of the dispersed elastomeric phase which is tantamount to the induced thermal stress. It was for the first time that the presence of such internal thermal stress is identified in rubber-modified thermoplastics. This may be a very important feature to guide blend development.

It has been demonstrated that the temperature dependence of v_{sp} of the PP's and the elastomers is quite different. This difference leads to volume dilatation of the blended elastomer between T_{cr}^{iPP}, T_{cr}^{sPP}, and T_g^{aPP}, respectively, and T_g^E. These dilatation effects occur in all PP blends, but they are most pronounced for iPP, as iPP has the highest crystallization temperature and the highest degree of crystallinity of the PP's. Not only the

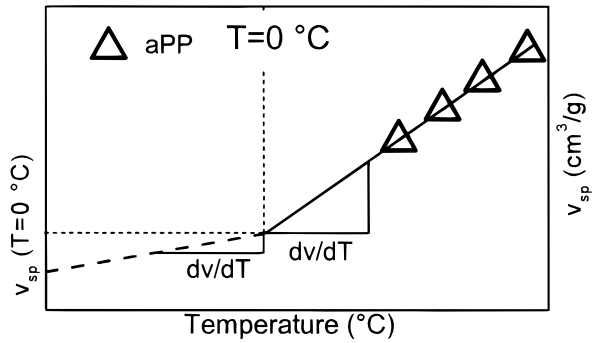

Figure 9. Scheme of determination of the slope dv/dT below $T_g^{PP} = 0$ °C.

structure, i.e., morphology, but also the thermal history and resulting internal thermal stresses govern mechanical properties of PP blends. It appears very likely that the thermally induced stress may also account for impact properties of PP/elastomer blends.

Acknowledgment. The authors thank the Bundesministerium für Bildung, Wissenschaft, Forschung und Technologie (project # 03D00551) for financial support and BASF AG, Ludwigshafen. Furthermore, the authors thank Prof. H. A. Schneider for intense discussion and helpful annotations.

Appendix: Extrapolation of v_{sp}

I. iPP, sPP, aPP. For all PP's the measured PVT data points between 30 and 60 °C were linearly fitted. Subsequently, the values of v_{sp} were extrapolated down to the $T_g^{PP} = 0$ °C by extending the determined linear fit. The expansion coefficient $\alpha(T \geq T_g)$ at $T_g^{PP} = 0$ °C (liquid state) was calculated according to $\alpha = v^{-1}(dv/dT)$ using the obtained value of $v_{sp}(T=0$ °C) and the slope (dv/dT) of the linear fit. The calculated values for $\alpha(T \geq T_g)$ at $T_g^{PP} = 0$ °C are α(iPP) $= 4.54 \times 10^{-4}$ K^{-1}, α(sPP) $= 5.84 \times 10^{-4}$ K^{-1}, and α(aPP) $= 7.46 \times 10^{-4}$ K^{-1} (α(aPP) is in good agreement with reported values[29,32,33]).

For aPP the $\alpha(T \leq T_g)$ (glassy state) was taken from the literature[29] as α(aPP) $= 1.87 \times 10^{-4}$ K^{-1} (application of the rule of Simha−Boyer[34] for amorphous polymers gives α(aPP) $= 3.32 \times 10^{-4}$ K^{-1}). Using this value of $\alpha(T \leq T_g)$ and $v_{sp}(T=0$ °C), the slope dv/dT for $T < T_g$ was calculated. v_{sp}(aPP) below T_g^{PP} from 0 to −50 °C was then computed using the slope dv/dT below T_g. Figure 9 illustrates the described procedure.

To calculate v_{sp}(iPP) of semicrystalline iPP at $T < T_g$, it is assumed that v_{sp}(iPP) at any temperature can be computed by a weighted linear combination of the v_{sp} of complete amorphous, v_{sp}(iPP,DC=0), and 100% crystalline iPP, v_{sp}(iPP,DC=1), using the degree of crystallinity, DC, as the weight factor.

$$v_{sp}(\text{iPP,DC}=0.6) = \text{DC}\,v_{sp}(\text{iPP,DC}=1) + (1 - \text{DC})\,v_{sp}(\text{iPP,DC}=0) \quad (2)$$

Taking into account that iPP has almost the same v_{sp} (and the same α) in the melt as aPP,[26] it can be assumed that at $T < T_{cr}$

$$v_{sp}(\text{iPP,DC}=0) = v_{sp}(\text{aPP}) \quad (3)$$

For the temperature range between 30 and 60 °C v_{sp}(iPP,DC=1) was calculated according to $v_{sp}(\text{iPP,DC}=1) = (v_{sp}(\text{iPP,DC}=0.6) - (1 - \text{DC})v_{sp}(\text{aPP}))/$ DC and linearly extrapolated to −50 °C. v_{sp}(iPP,DC=0.6) for $T < T_g$ was then calculated according to eq 2 using v_{sp}(iPP,DC=1) and v_{sp}(aPP) for $T < T_g$. The same procedure was applied to sPP neglecting the slightly different behavior of sPP in the melt compared to the cases of aPP and iPP.

II. SEBS, EO. Extrapolation of the v_{sp} of SEBS to −50 °C was realized by a linear fit through the measured data points in the range between 30 and 60 °C. The same extrapolation was not possible for EO as its melting temperature $T_m^{EO} = 60$ °C is too close to the lowest accessible temperature for PVT measurement. The curvature of v_{sp}(EO) did not allow a reliable linear fit.

References and Notes

(1) Utracki, L. A. *Polymer Alloys and Blends*, 1st ed.; Hanser Verlag: München, 1989.
(2) Collyer, A. A. *Rubber Toughened Engineering Plastics*, 1st ed.; Chapman & Hall: London, 1994.
(3) Goodier, J. N. *Trans. ASME* **1933**, *55*, 39.
(4) Wu, S. *Polymer* **1985**, *26*, 1855.
(5) Michler, G. H. *Kunststoff-Mikromechanik*, 1st ed.; Hanser Verlag: München, 1992.
(6) Cham, P. M.; Lee, T. H.; Marand, H. *Macromolecules* **1994**, *27*, 4263.
(7) Cimmino, S.; Guarrata, P.; Martuscelli, E.; Silvestre, C. *Polymer* **1992**, *32*, 3299.
(8) Schneider, H. A. In *Polymeric Materials Enyclopedia*, 1st ed.; Salomone, J. C., Ed.; CRC Press: Boca Raton, FL, 1996; Vol. 4, p 2777.
(9) Schneider, H. A. *J. Res. Natl. Inst. Stand. Technol.* **1997**, *102*, 229.
(10) Michler, G. H. *Plaste Kautschuk* **1988**, *35*, 423.
(11) Morbitzer, L.; Ott, K. H.; Schuster, H.; Kranz, D. *Angew. Makromol. Chem.* **1972**, *7*, 57. Kranz, D.; Morbitzer, L.; Ott, K. H.; Casper, R. *Angew. Makromol. Chem.* **1977**, *58/59*, 213.
(12) Schmitt, J. A. *IUPAC−Symposium*, Toronto, 1968, Reprints II, A9.
(13) Beck, R. H. *Polym. Lett.* **1968**, *6*, 707.
(14) Wu, S.; Bosnyak, C. P.; Sehanobish, K. *J. Appl. Polym. Sci.* **1997**, *65*, 2209.
(15) Suhm, J. Ph.D. Thesis, University Freiburg, 1998.
(16) Stricker, F.; Thomann, Y.; Mülhaupt, R. *J. Appl. Polym. Sci.* **1998**, *68*, 1891.
(17) Strobl, G. *The Physics of Polymers*, 2nd ed.; Springer-Verlag: Berlin, 1997.
(18) Moore, E. P. *Polypropylene Handbook*, 1st ed.; Hanser Verlag: München, 1996.
(19) Brandrup, J.; Immergut, E. H. *Polymer Handbook*, 3rd ed.; J. Wiley & Sons: New York, 1989.
(20) Zoller, P.; Bolli, P.; Pahud, V.; Ackermann, H. *Rev. Sci. Instrum.* **1976**, *47*, 948.
(21) Tait, P. G. *Phys. Chem.* **1888**, *2*, 1.
(22) Zoller, P.; Fakhreddine, Y. A. *Thermochim. Acta* **1994**, *238*, 397.
(23) Skorodumov, V. F.; Godovskii, Y. K. *Polym. Sci.* **1993**, *35*, 562.
(24) Setz, S.; Stricker, F.; Kressler, J.; Duschek, T.; Mülhaupt, R. *J. Appl. Polym. Sci.* **1996**, *59*, 1117.
(25) Lohse, D. J. *Polym. Eng. Sci.* **1986**, *26*, 1500.
(26) Maier, R.-D.; Thomann, R.; Kressler, J.; Mülhaupt, R.; Rudolf, B. *J. Polym. Sci., Polym. Phys.* **1997**, *35*, 1135.
(27) Bohn, L. *Angew. Makromol. Chem.* **1971**, *20*, 129.
(28) Eckstein, A.; Suhm, J.; Friedrich, C.; Maier, R.-D.; Sassmannshausen, J.; Bochmann, M.; Mülhaupt, R. *Macromolecules* **1998**, *31*, 1335.
(29) Van Krevelen, D. W. *Properties of Polymers*, 3rd ed.; Elsevier: Amsterdam, 1990.
(30) Galeski, A.; Piorkowska, E. *J. Polym. Sci., Polym. Phys.* **1983**, *21*, 1299, 1313.
(31) Wool, R. P. *Polymer Interfaces*, 1st ed.; Hanser Verlag: München, 1995.
(32) Wilski, H. *Kunststoffe* **1964**, *54*, 10, 90.
(33) Han, J.; Gee, R. H.; Boyd, R. H. *Macromolecules* **1994**, *27*, 7781.
(34) Simha, R.; Boyer, R. F. *J. Chem. Phys.* **1962**, *37*, 1003.

MA981154Q